SHORT CRACK PROPAGATION IN DUPLEX STEEL – EXPERIMENTAL CHARACTERIZATION AND MODELLING

O. Düber*, B.Künkler**, U.Krupp*, H.-J. Christ*, C.-P. Fritzen**
*) Institut für Werkstofftechnik, Universität Siegen
**) Institut für Mechanik und Regelungstechnik-Mechatronik, Universität Siegen
57068 Siegen, Germany
dueber@ifwt.mb.uni-siegen.de; kuenkler@imr.mb.uni-siegen.de

Abstract

The propagation behaviour of microstructurally short cracks in the duplex stainless steel 1.4462 has been examined. The different barrier effects of grain and phase boundaries were quantified by means of a *Hall-Petch* analysis, using results from fatigue experiments and measurements of the crystallographic orientation. Furthermore, by evaluating orientation data, the activated slip systems in individual grains could be identified. With this information two different crack propagation mechanisms (single slip/double slip) could be distinguished and correlated with different propagation rates.

A numerical model containing a mechanism-based description of the short crack propagation was validated by the observed cracks. The obtained quantities for the barrier effects are assigned to barriers that can be defined in the model. In addition, besides the algorithm for short crack propagation in single slip a new algorithm for simulating short crack propagation governed by a double slip mechanism is introduced. Comparisons between experimental data and simulation results have shown good agreement.

1 Introduction and theoretical background

In most cases, early crack propagation is determined by shear stresses on slip planes inclined by about 45° to the applied loading axis (under push-pull loading conditions), resulting in a zigzag-like crack path. Because of the strong interactions of short cracks with microstructural features (e.g. grain boundaries) and their substantially different growth mechanisms (stage I) compared to long cracks (stage II), the crack propagation rate da/dN of short cracks can not be described by linear elastic fracture mechanics (LEFM). Also the large plastic zone size, compared to the crack length, makes it necessary to use crack growth models based on elastic-plastic mechanics. Furthermore, the fact that short cracks can grow at higher rates than predicted from LEFM may lead to non-conservative design. Since the fraction of fatigue life which is determined by short crack propagation can reach up to 90% a model is required that is able to take the above-mentioned effects of microstructure on crack propagation into account.

1.1 Barrier effect of grain and phase boundaries

Grain and phase boundaries form obstacles for dislocation motion. The extent of this barrier effect depends on the nature of the boundary and can be quantified by a *Hall-Petch* analysis. The idea of *Hall* [1] and *Petch* [2] was, that plastic deformation on slip planes in front of a boundary leads to a pile-up of dislocations. This pile-up induces stress concentrations at the respective boundary as well as in the adjacent grain. If there are enough piled-up dislocations, the stress concentration on a dislocation source behind the boundary exceeds a critical value and dislocations can be emitted, i.e. the obstacle has been overcome and plastic deformation can spread out into the adjacent grain.

The original *Hall-Petch* relation describes the interrelation of the mean grain size and the yield stress, whereas the *Hall-Petch* constant k_y can be regarded as a measure for the resistance of a boundary against dislocation motion. In this form it is valid only for single phase materials and monotonic loading. Therefore, a modification for multi phase materials and cyclic loading was necessary.

According to *Fan et al.* [3], the extension on multiphase materials is described by the contributions of the different boundaries ($\alpha\alpha$–, $\gamma\gamma$–grain boundaries, $\alpha\gamma$-phase boundaries) to the yield stress, in connection with stereological parameters (which describe the geometrical arrangement of the different phases in the material). The resulting equation (1) allows to calculate the *Hall-Petch* constant for a phase boundary:

$$k_y^{\alpha\gamma} = \frac{(k_y^c - k_y^\alpha \cdot f_{\alpha c} - k_y^\gamma \cdot f_{\gamma c})}{F_s} \quad . \tag{1}$$

Here, k_y^x is the *Hall-Petch* constant for the respective boundary (k_y^c represents the two-phase material) and f_{xc} and F_s are stereological parameters. All factors on the right side can be determined experimentally. The numbers for k_y^x were defined by experiments with the respective materials (ferrite, austenite, duplex), the stereological parameters were obtained by image analysis of sections (in case of the single phase steels) and EBSD-Scans (in case of the duplex steel), respectively [4].

The extension on cyclic deformation was done just by replacing the monotonic yield stress in the *Hall-Petch* relation with the cyclic yield stress. This procedure is correct under the premise that planar glide prevails because only then a pile-up according to *Hall* and *Petch* can occur. Since most duplex steels are alloyed with nitrogen, which is known to assist planar glide, the application of the *Hall-Petch* idea to fatigue of duplex steels is justified.

1.2 Crack Propagation in single slip/double slip mechanism

The propagation behaviour of cracks can principally be divided into stage I and stage II. Stage I is characterized by a shear-controlled crack advance which takes place on slip planes showing a high *Schmid*-factor. In contrast, the stage II mechanism does not take place on a certain slip plane but perpendicular to the direction of the normal stress. According to *Neumann* [5], the crack path is assembled from alternatingly-operated slip systems.

The reason for the two different growth mechanisms is, that at the beginning of crack growth (stage I) the crack length and hence, the stress concentration at the crack tip is relatively small. It is not high enough to activate additional dislocation sources on other slip planes than the already operating one. Only when the crack has reached a certain length, additional dislocation sources can be activated, whereas this length depends on the geometrical location of the slip planes to each other and the global stress. Then the above mentioned alternating slip is possible, like it occurs in stage II long crack propagation. Since this paper is dealing with short cracks it is inappropriate to speak of stage II. In order to avoid misunderstandings the terms *single slip* and *double slip* have been chosen in the following sections.

2 Experimental

2.1 Material

As testing material the austenitic-ferritic duplex stainless steel with the German designation 1.4462 was chosen. For the examinations concerning the barrier effect of boundaries the single phase austenitic (1.4404) and ferritic (1.4511) steels were available. Their chemical composition is given in Table 1.

TABLE 1: Chem. Composition of the examined steels (Wt%)

	Fe	Cr	Ni	Mo	Mn	Si	Nb	N	C
1.4462	bulk	21,9	5,6	3,1	1,8	0,5	-	0,1871	0,020
1.4404	bulk	16,6	11,1	-	1,3	0,6	0,01	0,0296	0,018
1.4511	bulk	16,3	-	-	0,7	0,5	0,253	-	0,012

In the as-received condition the duplex steel is hot rolled and solution annealed at 1050°C. As a result of the rolling process, austenite and ferrite are present in the form of long lamellae. For better detection of microcrack propagation the fine-grained microstructure was heat treated (1250°C, 4h) in order to coarsen it. This lead to an increase in the α/γ-ratio which was initially around 0.5. After four hours the temperature was lowered to 1050°C within three hours, which shifted the α/γ-ratio back to 0.5. To reduce residual stresses a final annealing at 550°C for 45 min was added.

2.2 Experimental methods

Fatigue experiments were conducted at room temperature using a servohydraulic testing system MTS 810. The cyclic yield stresses for the *Hall-Petch* analysis were obtained by plastic-strain-controlled incremental step tests on austenitic, ferritic and duplex steel specimens with different mean grain sizes. The plastic strain rate was $\dot{\varepsilon}_{\mathrm{pl}} = 5 \cdot 10^{-4}\,\mathrm{s}^{-1}$.

The fatigue experiments for crack growth characterization were done in normal stress control with different stress amplitudes, a stress ratio of R=-1 and a frequency of f=1Hz. The tests were interrupted periodically after constant intervals and the specimen surface was searched for nucleated and propagated cracks in the SEM.

Crystallographic orientations were measured by means of the EBSD-technique (*electron backscattered diffraction*) in combination with OIM™ software (*orientation imaging microscopy*) in the SEM. The application of EBSD requires a flat surface free of residual stresses, wherefore the specimens were polished electrolytically prior to fatigue testing.

The stereological parameters are achieved by image analysis of EBSD-Scans (in case of the two phase duplex steel) or etched sections (in case of the single phase steels), respectively.

3 Results

3.1 Barrier effect of grain and phase boundaries

Fig. 1 shows the results of the barrier effect experiments for the different boundaries in form of a *Hall-Petch* plot (cyclic yield stress vs. reciprocal square root of mean grain/cluster size). Obviously, the duplex steel has the highest yield stress of the three steels. This can be explained by the lamellar structure of the phases originating from the rolling process. Perpendicular to the lamellae the material has a high resistance against slip transmission since a lot of boundaries have to be passed. This leads to a high yield stress for loading in parallel direction to the lamellae and hence, the duplex steel can be regarded as a sort of composite material.

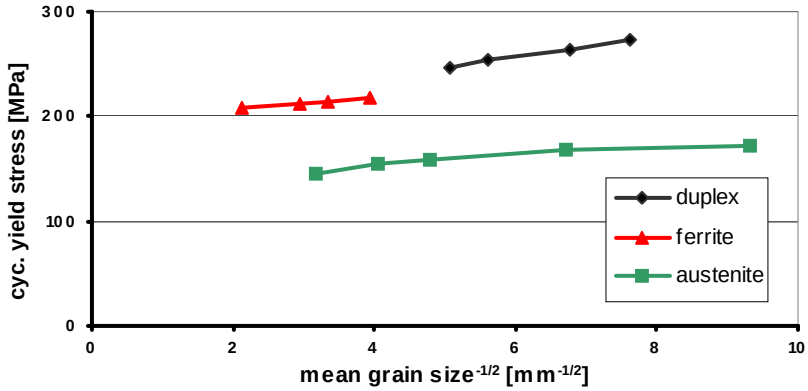

FIGURE 1: Hall-Petch plot of the results from the Incremental Step Tests

The slope of the lines in Fig. 1 represents the corresponding *Hall-Petch* constants and with it a measure for the barrier efficiency of grain and phase boundaries. Here again, the duplex steel exhibits the highest value. Since the cyclic yield stress of the duplex steel results from the contributions of grain and phase boundaries the measured factor is a mixed value. The value for a single phase boundary can be calculated by applying equation (1) and is given in Table 2, together with the corresponding data for αα- and γγ-grain boundaries. Also the friction stress of the different phases, which here is termed *microstructural cyclic yield stress* (for the movement of dislocations) can be found.

TABLE 2: Results of the *Hall-Petch* experiments

	γγ	αα	αγ	**Duplex**
microstructural cyclic yield stress $\sigma_{fl,c}$[MPa]	137	198	212	196
Cyclic *Hall-Petch* constant k_c[MPa$\sqrt{\text{mm}}$]	4.2	5.0	15.8	10.1

3.2 Single slip/ double slip crack propagation

Short crack growth in the examined duplex steel takes place in two different deformation mechanisms. On the one hand cracks grow along one slip band (single slip), on the other hand crack growth occurs by the previously mentioned *Neumann*-mechanism by alternatingly operating slip systems (double slip). The resulting assembled crack path can be calculated with orientation data.

Fig. 2 shows two examples for the different ways of propagation. Fig. 2a shows a short crack, which has initiated at a twin boundary. The solid lines refer to parts of the crack paths where the crack has grown in single slip on the indicated slip systems (between points ①,② and ⑤,⑥). The dashed lines label parts in the crack path where the crack has grown by alternating operation of two slip planes. Between points ③,④ and ④,⑤, respectively, the crack grew by activating the (111) and $(\bar{1}11)$ slip planes. At point 4 there is a transition from a inclined to a horizontal path (perpendicular to the applied stress axis). The reason for this is, that between ③,④ the involved slip planes contribute to the crack advance in equal parts, while between ④,⑤ the slip on the (111) plane is as twice as high as on the $(\bar{1}11)$ plane. A calculation shows that this should change the angle between the crack path and the horizontal direction from –19° to 3°, what indeed can be found on the micrograph.

In Fig. 2b, another example is given. Between ①,② crack growth results from the operation of different single slip systems, while between ②,③ again the denoted slip systems (111)

and $(\bar{1}11)$ are activated alternatingly. Under the assumption that slip on the (111) plane is twice as high as on the $(\bar{1}11)$ plane, the calculation yields an angle of approximately –1° between the crack path and the horizontal direction and here also these angles can be found on the micrograph.

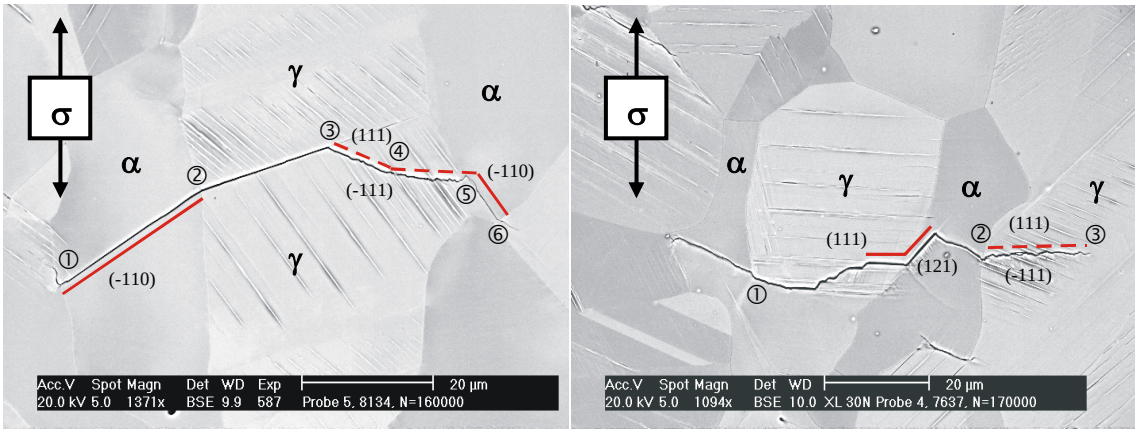

FIGURE 2: Crack paths of some short cracks

a) Δσ/2=370MPa, N=160,000 b) Δσ/2=400MPa, N=170,000

For the two different growth mechanisms one can find different growth rates. Fig. 3 again shows the two cracks from Fig. 2. Labelled is the original crack after 50,000 cycles. The spacing between the vertical markings show how far the crack has travelled after equidistant numbers of 10,000 cycles. As can be seen in Fig. 3a, the crack grows faster in single slip (between ①,② and ⑤,⑥) than in double slip. The same is true for the crack shown in Fig. 3b between ①,② (single slip, fast growth) and ②,③ (double slip, slow growth).

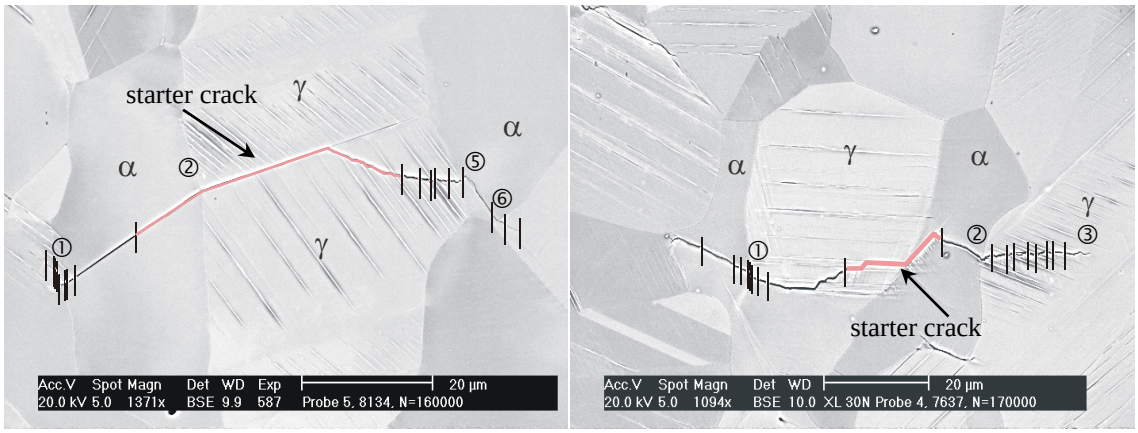

FIGURE 3: Crack propagation of some short cracks

a) Δσ/2=370MPa, N=160,000 b) Δσ/2=400MPa, N=170,000

4 Numerical crack growth simulation

4.1 The model

In the following, the model and some recent extensions are briefly presented. The model describes a slip band consisting of a series of slip band pieces. The slip band allows relative tangential displacements of the slip band faces against each other, which after *Hills et al.* can be described by edge dislocations [6]. In the model, “mathematical” dislocations instead of

physical dislocations are used to represent a displacement discontinuity. Plastic deformation is described by these dislocations and occurs if the shear stress on the slip band exceeds the resistance of dislocations to motion. A crack is defined as that part of the slip band which, in contrast to the rest of the slip band, is allowed to open. The opening of the crack is modelled by additional "mathematical" dislocations perpendicular to the slip band. Hence, the crack and its plastic zones are represented by an arrangement of dislocations. Additionally, so-called "sensor elements" are introduced, which can be used to determine the state of stress at any position.

By use of a boundary element method (which's elements consist of the above mentioned mathematical dislocations), the displacements in the crack and its plastic zones can be calculated. Analogous to the model of *Navarro* and *de los Rios* [7], the current crack propagation rate d*a*/d*N* is determined by means of the power-law function

$$\frac{da}{dN} = C \cdot \Delta CTSD^m \quad . \tag{2}$$

Here $\Delta CTSD$ is the range of crack-tip slide displacement, C is a material-specific constant and m is an exponent. For a more detailed description of the model, see *Schick* [8] and *Kuenkler et al.* [9].

4.2 Verification

In order to verify the crack propagation model it was applied to cracks that were observed during fatigue experiments. The starter crack obtained in the experiment undergoes a cyclic loading calculation and the geometry of the crack was defined by the actual crack path. The examples in Figures 4a and 4b show the simulated crack length versus cycles in comparison with experimental data.

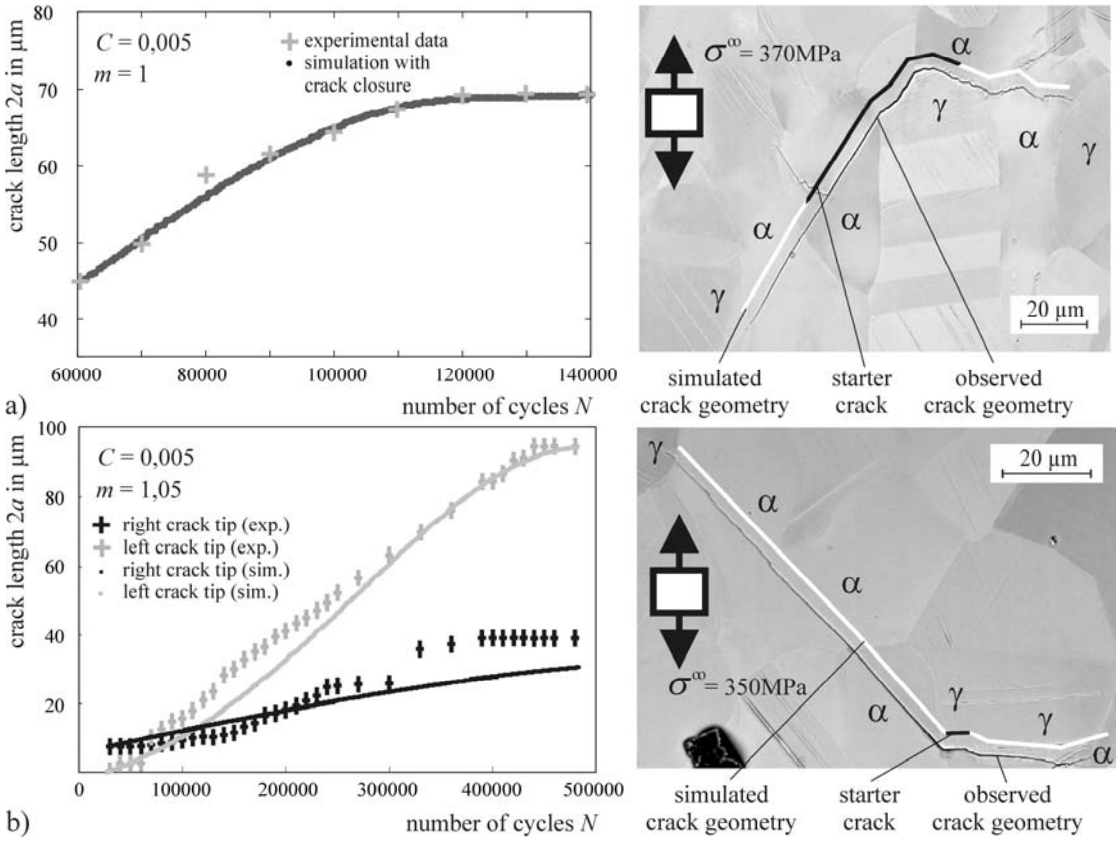

FIGURE 4: Comparison simulation/experiment for two short cracks

In Figure 4a, the experimentally-observed deceleration of the left crack tip can be attributed to the dislocation pile-up at the phase boundary. This could be quantitatively simulated. The crack can propagate through the boundary only if the shear stress on a slip plane in the neighbouring grain, represented by a sensor element, exceeds a boundary-dependent critical value. In Figure 4b, the calculated crack growth rate of the left and right crack tip also fits to the experimental data. The difference in the calculated crack growth rates of the two tips is due to the difference in the resistance to shear deformation in the individual phases and due to the difference in the shear stresses acting on the crack planes, which depend on the orientation of the crack paths with respect to the loading axis. This has a strong impact on the range of crack tip slide displacement and thus the crack growth rate.

4.3 Transition from single slip to double slip

To simulate the transition of crack growth on single slip planes to crack growth on multiple slip planes, a stage I crack inclined by about 45° to the applied loading axis is simulated (Fig. 5a). Fig. 5b shows the shear stress distribution around the crack tip in a constant radius for a linear elastic crack (grey) and a linear elastic-plastic crack with plastic deformation on one slip plane only (black).

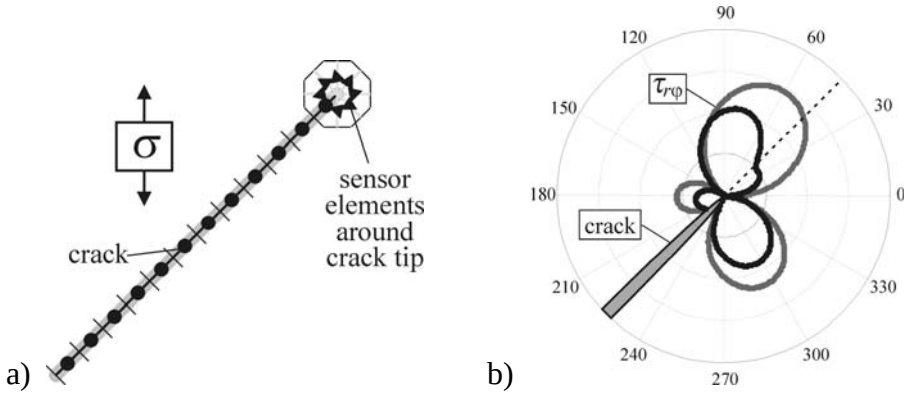

FIGURE 5: Elastic crack with additional sensor elements (a) and shear stress distribution around crack tip (b).

The stresses are calculated by the mentioned boundary method with sensor elements around the crack tip (Fig. 5a). The calculated elastic stress distribution is identical to the analytical solution. The stress distribution for the elastic-plastic calculation exhibits a decrease of the shear stress near the slip plane until the plastic shear stress is reached. In larger distance to the plastic deformation, the shear stress is nearly as high as for the elastic crack. Thus, for crack simulations in microstructures additional sensor elements representing other slip planes of the grains are positioned at the crack tip to determine the shear stress on those slip planes (Fig. 6a). If a critical stress value on one of these sensor elements is reached, the additional slip plane is considered to be activated and plastic deformation can occur on this second slip plane (Fig. 6b). This is in accordance to *Lin* and *Thomson* [10], who claim that a certain stress intensity has to be reached to activate additional slip systems in front of the crack tip.

After the activation of the second slip plane, the new crack-tip position results from the composition of the plastic slip vectors. New sensor elements are now positioned at the new crack tip representing new slip planes and again these elements are activated (Fig. 6c), whereas the plastic deformation on the previous slip planes is considered. With growing crack length, the crack is deflected on a path perpendicular to the loading axis, and a crack propagation perpendicular to the direction of the maximum normal stress occurs (like for

long cracks in stage II, Fig. 6d). If the orientations of the slip planes change (because the crack tip has reached a new grain) and the crack is still relatively short, the crack possibly grows again on a single slip plane because no adequate second slip plane is available. This is in accordance with experimental observations (see Fig. 2a after point 5).

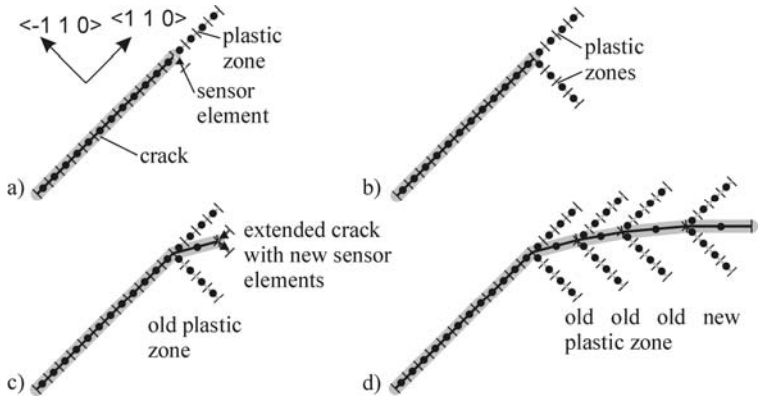

FIGURE 6: Transition from single slip to multiple slip

5 Conclusions

An approach to quantify the barrier effects of different kinds of boundaries and the microstructural cyclic yield stress was presented. Furthermore, two different propagation mechanisms (single/double slip) could be identified. The values obtained experimentally were implemented into a numerical model for the simulation of stage I crack propagation. This model is able to describe the impact of microstructure on short crack growth like crack deceleration in front of barriers and other important phenomena (crack closure and geometrical arrangement of the microstructure, as it is shown elsewhere [11]) in a mechanism-oriented way.

The extension on the transition single slip/double slip allows to simulate the damage evolution under cyclic loading from a short starter crack onward to a crack, which is independent from microstructure, whereas the crack advance is reproduced in a physically reasonable way.

6 References

1. Hall, E.O., *Proc. Phys. Society London B*, **64** (1951) 747
2. Petch, N.J., *Iron Steel Inst. B*, **174** (1953) 25
3. Fan, Z., Tsakiropoulos, P., *Phil. Mag. A*, **67** (1993) 515
4. Krupp, U., Düber, O., Christ, H.-J., Künkler, B., Schick, A., Fritzen, C.-P., *Journal of Microscopy*, **213** (2004) 313
5. Neumann, P., *Acta Met*., **22** (1974) 1155
6. Hills, D.A., Kelly, P.A., Dai, D.N., Korsunsky, A.M., *Solution of crack problems*, Kluwer Academic Publishers, London, 1995
7. Navarro, A., de los Rios, E.R., *Phil. Mag. A*, **57** (1988) 15
8. Schick, A., *Ein neues Modell zur mechanismenorientierten Simulation der mikrostrukturbestimmten Kurzrissausbreitung*, doctoral thesis, Universität Siegen, 2004

9. Künkler, B., Schick, A., Fritzen, C.-P., Floer, W., Krupp, U., Christ, H.-J., *Steel Research*, **74** (2003) 514

10. Lin, I.H., Thomson, R., *Acta Met.*, **34** (1986) 187

11. Düber, O., Künkler, B., Krupp, U., Christ, H.-J., Fritzen, C.-P., in *Proc. Mechanismenorientierte Lebensdauervorhersage für zyklisch beanspruchte metallische Werkstoffe*, DVM-Bericht 685, Bremen (2004) 69